Measuring the electronic corrugation at the metal/organic interface

Benjamin W. Caplins, Alex J. Shearer, David E. Suich, Eric A. Muller, and Charles B. Harris*
Department of Chemistry, University of California at Berkeley, Berkeley, California, USA
and Chemical Sciences Division, Lawrence Berkeley National Laboratory, Berkeley, California, USA
(Received 16 December 2013; revised manuscript received 13 March 2014; published 21 April 2014)

Angle-resolved two-photon photoemission is used to probe the image potential states on monolayers of metal-free phthalocyanine (H_2Pc) and cobalt phthalocyanine (CoPc) on the Ag(100) and Ag(111) surfaces. We find that in the plane of the surface the normally flat potential landscape becomes significantly corrugated in the presence of the phthalocyanine lattice, causing the opening of a band gap in the first image potential state, in agreement with previous findings. Interestingly, the data show that the absence of the electron dense metal center does not qualitatively alter this picture. Experiments conducted on Ag(100) and Ag(111) crystals demonstrate that the surface band structure and symmetry of the metal surface plays a minor role in the band folding phenomenon. A two-dimensional model that takes into account both the band structure of the substrate and the corrugation of the potential landscape in the surface plane due to the molecular lattice is presented and compared to experiment. This model enables the observation that, counter to intuition, the Co metal center at the CoPc/Ag interface actually smooths the interfacial potential relative to that of the H_2Pc/Ag interface. We suggest that the strong corrugation of the potential at the organic/metal interface measured herein may account for the recent observation of surface umklapp scattering in recent ultraviolet photoemission experiments on organic/metal interfaces.

DOI: 10.1103/PhysRevB.89.155422 PACS number(s): 79.60.Dp, 73.20.At

I. INTRODUCTION

Metal-organic interfaces are critical to understanding the behavior of organic electronic devices due to their role in charge injection/collection in organic light-emitting diodes and organic photoconductors [1–4]. The electronic structure and interfacial potentials at these interfaces control the charge injection barrier and efficiency of these processes. Frequently, the spatial organization at the metal-organic interface is poorly defined and thus is not explicitly considered in the resulting electronic structure. Here, we use the image potential states [5–7] (IPS) as probes to show that the potential energy surface at the popular phthalocyanine/Ag interface is highly corrugated, resulting in a modified interfacial electronic band structure.

At metal/molecule interfaces, the electronic states that commonly dominate the spectra are the image potential states (IPS). The IPS arise from the attractive force an electron experiences outside of a dielectric material due to an induced polarization. Energetically, the IPS form a Rydberg series perpendicular to the surface plane given by the equation

$$E_n = \frac{-0.85\text{eV}}{(n+a)^2} + V_0,$$

where n is the principal quantum number and a is the quantum defect parameter, and V_0 represent the vacuum energy. The first few wave functions are localized to within a few angstroms of the interface [Fig. 1(a)]. This spatial location of the IPS makes them sensitive to the static and dynamic properties of the interface's potential energy landscape. Previous studies have used IPS to monitor phenomena as diverse as the dynamic collapse of electronic wave functions in organic solvents [8–10], the creation of coherently controlled electric currents [11], and the formation and evolution of quantum well states in noble gas thin films [12,13].

Perpendicular to the surface the IPS are bound, but parallel to the surface they are typically thought to experience an essentially flat potential [14] resulting in a continuum of electronic states indexed by an electron wave vector $k_{||}$ [Figs. 1(c)–1(d)]. These states form a parabolic band with an effective mass close to that of a free electron. Due to the range of $k_{||}$ values experimentally accessible and the intrinsic lattice constants of most previously studied systems, strong deviations from a parabolic band dispersion are uncommon in two-photon photoemission (TPPE) spectra; the known exceptions to this involve dynamic nuclear or electronic events such as small polaron formation [9] and electron localization [10], which are unlikely to occur in the present system. Lattice constants in many organic semiconductors are much larger, however, on the order 10–20 Å, and the approximation of a featureless potential becomes less robust. Instead, the lattice can interact strongly with and spatially confine the Bloch wave functions [15]. This results in an altered electronic band structure with a forbidden energy gap of width Δ, which splits the single parabolic band into multiple "back-folded" bands, which here are distinguished from the unperturbed $n = 1$ IPS and labeled as the $n = 1_A$ and $n = 1_B$ states [Figs. 1(e)–1(f)].

Until recently, this type of IPS/molecular lattice interaction was observed only through the lowest band denoted $n = 1_A$ via the observation of an effective mass greater than that of a free electron and the observation of the band folding downwards in energy at the edge of the first Brillioun zone [16–20]. Never was the interaction strong enough to observe the $n = 1_B$ state. Recently, however, the $n = 1_B$ state was clearly observed upon the deposition of copper phthalocyanine (CuPc) and iron phthalocyanine (FePc) monolayers on Ag(111) and lead phthalocyanine (PbPc) monolayers on highly ordered pyrolytic graphite (HOPG) [21,22]. This effect was modeled via a periodic square-well model where it was assumed that the difference in the electronic screening of the π system of the phthalocyanine core and the σ bonds of the molecular periphery caused a substantial corrugation felt

*cbharris@berkeley.edu

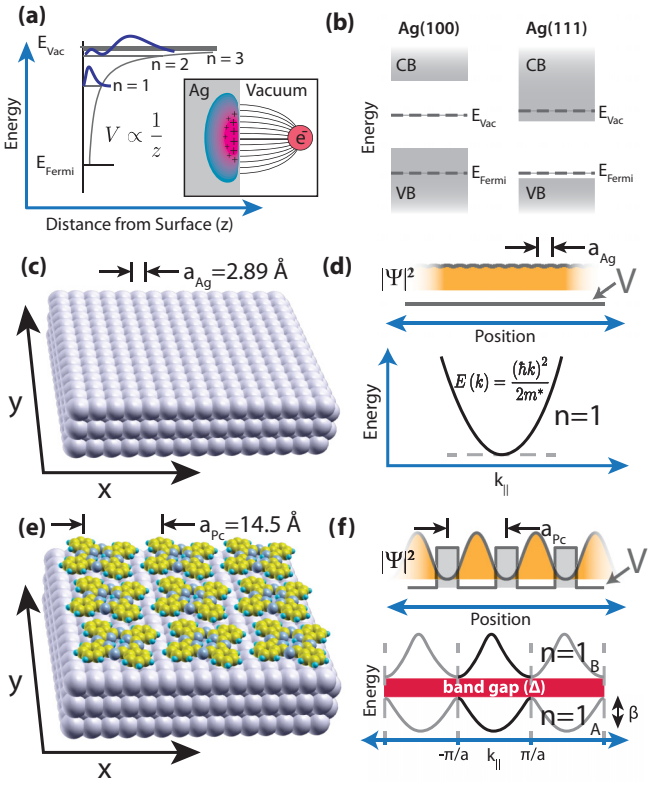

FIG. 1. (Color online) (a) Image potential state progression outside of a metal surface. The first two wave functions are drawn. The inset shows the interaction of an electron with a metal surface. (b) Surface projected bulk band structure at $k_{||} = 0$ for the Ag(100) and Ag(111) surfaces. The image potential states are just below the vacuum level, and are thus mid-gap on Ag(100) and at the top of the gap on Ag(111). (c) The bare silver surface and (d) the corresponding (flat) potential energy surface, (nearly constant) wave function, and free-electron-like band dispersion parallel to the surface. (e) The phthalocyanine covered silver surface and (f) a simple square-well potential energy surface, resulting wave function, and band dispersion parallel to the surface. Note the strong periodic corrugation of the potential, and the band gap that it opens in the surface band structure.

by the image potential electron. This model was shown to adequately explain the experimental results including intensity and symmetry considerations.

In this study, we attempt to understand the origin of the band folding in phthalocyanine molecules and how it presents in TPPE spectra. Characterizing the way it manifests in spectra and understanding the forces that cause it are necessary for the full interpretation of TPPE spectra of phthalocyanines and materials that have lattices on the appropriate length scale. Additionally, analyzing the band folding in TPPE spectra allows us to back out a quantitative understanding of the interfacial potential energy landscape which is interesting to a broad audience. For example, the tailoring of the electronic properties of graphene via a PTCDA superlattice [23], or the full understanding of recent photoemission experiments that have noted strong umklapp type scattering of bulk metal states by phthalocyanine based lattices [24–26]. We suggest that the band folding seen in our experiments and the scattering seen in the photoemission experiments are derived from a common origin.

Specifically we investigate the following. (1) What is the role of the metal center? The simplest picture would suggest that the electron density from the metal center would cause an increase in the potential corrugation and lead to enhanced band folding. To answer this, we compare cobalt phthalocyanine (CoPc) and metal-free phthalocyanine (H_2Pc) molecules in order to discern the effect of the metal center on the spectra. This study might suggest methods for tuning the strength of the potential corrugation. (2) What effect does the substrate have on the band folding? Ag(100) and Ag(111) surfaces were used to determine the role of the substrate surface projected bulk band structure and the surface symmetry in determining the band folding in the observed image potential states. (3) Are the phthalocyanine based ligands unique in their presentation of the band-folding phenomenon, or is the effect more general? To answer this question, we compare the phthalocyanine data to data from the model PTCDA/Ag(100) interface. This system is convenient because it is known to grow in large, highly crystalline domains with a known unit cell of appropriate dimension [27]. This system will test whether or not the lattice constant and crystallinity are the primary factors influencing the observation of band folding, or if other factors such as the molecular charge distribution are at work. The systematic study of multiple well-characterized molecules on two different silver surfaces should form a substantially clearer picture of how band folding manifests in TPPE experiments.

Finally, because no rigorous electronic structure calculation is capable of modeling these back folded states *ab initio*, we construct a simple model that reproduces the experimental spectra and captures the relevant physics. This model takes into account the bulk band structure, the effective electron affinity of the adlayer, and the corrugation of the interfacial potential. The model data are compared with experiment and reasonable agreement is found, yielding a method to measure of the magnitude of the corrugation of the interfacial potential.

II. EXPERIMENTAL

Experiments were performed in an ultra-high vacuum chamber with a base pressure of $<5\times10^{-10}$ Torr. Samples were heated resistively up to 750 K or cooled with a liquid nitrogen cryostat to 120 K. The Ag(111) and Ag(100) crystals were purchased (Princeton Scientific) in >99.999% purity and cut to $<1^\circ$ accuracy. Cleaning of the Ag(111) [Ag(100)] surface was performed by Ar^+ sputtering with the sample held at 500 K (500 K) and subsequent annealing to 725 K (675 K). Cleanliness and order was verified by low-energy electron diffraction (LEED), Auger electron spectroscopy (AES), and TPPE.

Samples of CoPc and H_2Pc were obtained in >97% and >98% purity (Sigma), respectively, and degassed in ultrahigh vacuum for several days at elevated temperatures. Material deposition was accomplished from pyrolitic boron nitride crucibles by commercial effusion cells. During material deposition the analysis chamber was kept $<10^{-9}$ Torr. High-quality monolayer films of H_2Pc/Ag(100), H_2Pc/Ag(111), and CoPc/Ag(111) were prepared by multilayer deposition and subsequent annealing for maximum signal to noise as measured by a combination of TPPE and LEED. It was found that the CoPc/Ag(100) and PTCDA/Ag(100) films prepared in

this way had undesired unit cells as seen by LEED, so these layers were prepared by carefully metered dosing.

A commercial Ti:Sapphire laser system operating at 297 kHz was used in the TPPE experiments [28]. The output of this system was tunable through visible wavelengths, and was compressed to <100 fs. A portion of this output was frequency doubled in a 250-μm BBO crystal and after a delay stage the UV and Vis pulses were combined and focused onto the sample, forming the pump and probe for the TPPE experiments. All experiments were performed at 120 K in order to maximize the signal to noise. No photodegradation was detected for these materials. Measurements on the clean Ag(111) crystal of the surface state resulted in a cross correlation width of ∼120 fs.

In this work, we use TPPE to examine the interfacial potential landscape present at the metal/organic interface. Briefly, TPPE is a pump-probe technique [29,30] where a pump pulse excites an electron from below the Fermi level of the metal substrate into an intermediate unoccupied state. An optically delayed probe pulse photoemits the electron into the vacuum where it is detected by a time-of-flight electron detector. In our implementation of this technique, the probe pulse is the output of a visible optical parametric amplifier and the pump pulse is the frequency double of the probe. This technique has an energy resolution of <20 meV and the time resolution is limited by the ∼120 fs cross correlation between the pump and probe pulse. Momentum resolved TPPE experiments were performed by rotating the substrate with respect to the detector with ∼3° resolution along the $\bar{\Gamma}$-$\bar{K}_{Ag(111)}$ and $\bar{\Gamma}$-$\bar{X}_{Ag(100)}$ directions for the Ag(111) and Ag(100) surfaces, respectively. The presence of several rotational domains on the phthalocyanine/Ag(111) surface causes several directions to be probed simultaneously, the effect of which is clarified on the phthalocyanine/Ag(100) surface, which has high-symmetry lines parallel to those of the substrate. The $\bar{\Gamma}$ point was located as the energetic minimum of the dispersive clean silver states. Least-squares fitting was used to accurately extract peak locations; Voight functions were used to model IPS, and an exponential multiplied by a Fermi-Dirac distribution was used to model the background.

III. RESULTS

A. Preparation and characterization of monolayer films (LEED)

The adsorption of phthalocyanine molecules have been studied previously on many noble metal surfaces including the Ag(100) [31–33] and Ag(111) [34–43] surfaces. On close packed noble metal surfaces, the phthalocyanine ligands are known to adsorb parallel to the metal surface in either a Frank-van der Merve or Stanski-Krastanov growth mode. The molecules are known to be mobile at room temperature and large crystalline domains can be grown using slow deposition rates and elevated substrate temperatures. Homogenous monolayers can be grown via multilayer deposition and subsequent annealing above the multilayer desorption temperature. It should be noted here, however, that although this strategy of annealing multilayers can lead to a uniform monolayer coverage, the surface lattice obtained in such a way may not match up to that observed by carefully metered dosing.

For the H_2Pc/Ag(111) surface, the point-on-line monolayer structure was formed directly upon desorption of the multilayer as noted previously [36]. The CoPc/Ag(111) surface formed with a nearly identical surface lattice, which was unsurprising given that the CuPc/Ag(111) [37] and SnPc/Ag(111) [38] surfaces also pack in this manner. On the Ag(100) surface, we were interested in preparing the 5 × 5 commensurate structure [33]. For the H_2Pc/Ag(100) surface, this structure was not reached upon multilayer desorption. Instead, it was prepared most easily and reproducibly by reducing the monolayer density by annealing to 620 K. The same procedure was attempted for CoPc/Ag(100), but for annealing temperatures as high as 650 K it did not yield the desired structure, instead it favored a LEED pattern with an identical lattice constant, but rotated with respect to the Ag lattice. To avoid this issue, the 5 × 5 commensurate phase of CoPc/Ag(100) was prepared by carefully metered dosing. The PTCDA/Ag(100) layer was also prepared this way because desorption of the multilayer led to a structure similar to the herringbone structure seen previously only in multilayers, as opposed to the T-shaped structure where the long molecular axis line up with the Ag(100) high symmetry lines [27].

Representative LEED images of the interfaces studied are shown in Fig. 2. Figures 2(a) and 2(c) each show the CoPc and H_2Pc spectra side-by-side for both substrates for the same beam energy, clearly demonstrating that *the layer structure and quality are similar for both surfaces*, which is critical for any quantitative comparison of their electronic structure.

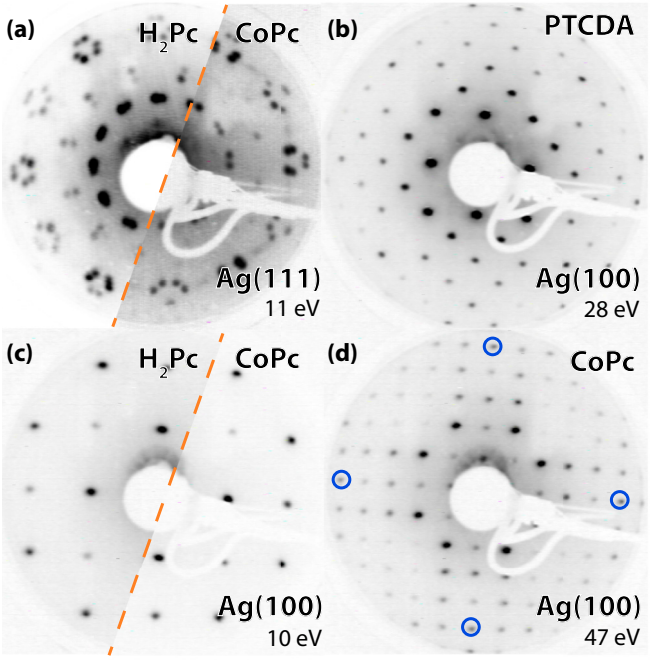

FIG. 2. (Color online) LEED images of the organic monolayers studied herein, taken at the beam energies indicated. (a) Previously reported point-on-line pattern on both H_2Pc/Ag(111) and CoPc/Ag(111). (b) The known $c(8 \times 8)$ PTCDA/Ag(100) structure. (c) The 5 × 5 H_2Pc/Ag(100) and CoPc/Ag(100) structures used in this study, with (d) showing the substrate spots circled in blue.

B. Two-photon photoemission spectra

The TPPE spectra resulting from desorption of the multilayer or metered dosing of the monolayer are all qualitatively identical and are dominated by an intense peak at low kinetic energies and several weaker peaks approximately 0.7 eV higher in energy, as shown in Fig. 3(a). In order to determine the location of these peaks with respect to Fermi and vacuum reference levels, the work function was measured via the onset of one-photon photoemission and a wavelength survey was performed. In the wavelength survey, shown in Fig. 3(a), the pump and probe pulse energies are varied in order to determine which laser pulse photoemits the electron. The resulting fits to the peak positions are plotted versus photon energy and a slope of one clearly indicates the visible pulse is responsible for photoemitting the electrons [see Fig. 3(a) inset]. In conjunction with the work function measurement, this allows for a determination of the binding energies of the peaks with respect to the vacuum energy.

The energetic locations of these peaks and their relative intensities point to them being a Rydberg series of image potential states [5]. Spectra taken at a time delay seen in Fig. 3(b) also confirm this assignment, as it is seen that the states at high kinetic energy are longer lived than those at low kinetic energy and are thus decoupled from the surface as expected for an IPS series. This assignment then allows for a more accurate determination of the states' binding energies. In all cases, the first three image potential states were fit to a Rydberg series leaving the quantum defect and vacuum level as free parameters. This allowed very accurate determination of the binding energies of the states [44]. It should be noted that including higher quantum number states and/or excluding the first image potential state from the fit had only a very minor effect on the resulting vacuum energy, on the order of 10 meV, which set the lower limit on the error in the binding energies. The resulting binding energies are summarized in Fig. 3(c).

It may be noted that the strongest bound IPS for the H_2Pc/Ag(100) layer has a wider asymmetric line shape, which is most likely attributable to the difference in layer preparation for that system; the annealing step for that system was carried out at 620 K in order to lower the monolayer molecular density and attain the 5×5 commensurate structure. The LEED images indicate a highly-ordered structure, and the existence of the Rydberg series (observed up through $n = 4$ for $t > 0$ time delays) suggests a uniform surface suitable for dispersion measurements.

C. Angle-resolved measurements

Angle-resolved two-photon photoemission spectra probe different slices in k space, directly measuring the interfacial band structure. Angle-resolved data collected on the interfaces under study are shown in Fig. 4. The spectra were all normalized to have equal maximum intensity to aid in visualization of the peak locations at all angles. The most obvious feature to note is that all the phthalocyanine spectra, Figs. 4(a)–4(d), are qualitatively identical. The states that were assigned to the IPS states all shift to lower binding energy as the crystal is rotated from normal emission geometry consistent with free electron like nature of image potential states. In addition to these states, however, in all cases, a peak is seen to increase

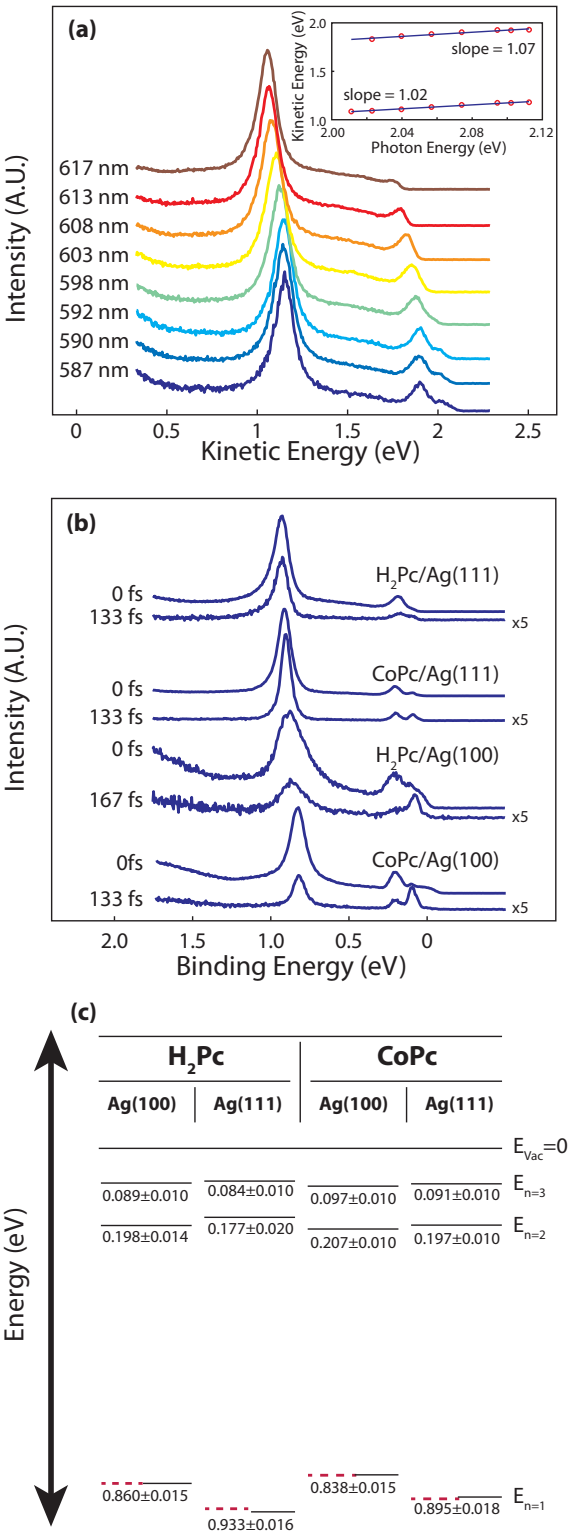

FIG. 3. (Color online) Two-photon photoemission (TPPE) spectra of the H_2Pc/Ag(111) surface at several different probe photon energies. The inset shows that the probe photon had energy $h\nu$ and allows for intermediate state energy assignment. (b) TPPE spectra showing the image potential state structure. Spectra at positive delays are shown scaled by x5 in order to clearly distinguish the $n = 3$ states. (c) The energy level diagram of the systems studied given in binding energy. Note the red dotted lines were calculated from the one-dimensional electron affinity model (see below).

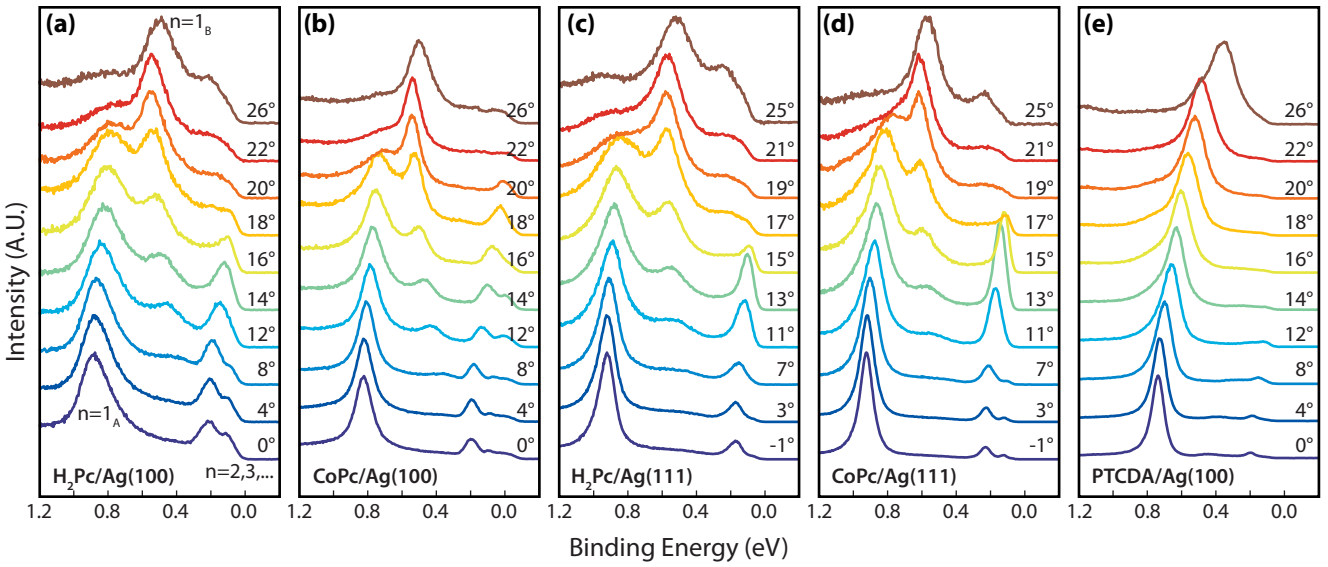

FIG. 4. (Color online) Angle-resolved TPPE spectra collected on the surfaces under study. Spectra are plotted versus binding energy with respect to vacuum, and have been normalized to have equal maximum peak height for better visualization of peak locations. For the phthalocyanine data (a)–(d), the $n = 1_A$ and the $n = 1_B$ states are the dominant peaks at approximately 0.85 and 0.5 eV, respectively; these states are explicitly labeled in (a). For the PTCDA data, (e), only the $n = 1$ state has measureable intensity.

in relative intensity with increasing angle with an energetic position between the $n = 1_A$ and $n = 2$ IPS. This is assigned to the back-folded $n = 1_B$ band by comparison with the literature [21,22]. Additionally, a small peak is observed at very high angles near 0.2-eV binding energy; this peak will be briefly discussed later.

Figure 4(e) shows a dispersion from the PTCDA/Ag(100) surface. In this case, three peaks can be distinguished. The peaks at 0.74 and 0.20-eV binding energy are assigned to the $n = 1$ and $n = 2$ IPS, respectively. They are seen to decrease in binding energy with increasing angle in a continuous manner. Only in the 26° spectra does the line shape obviously change. Most strikingly, no state grows in intensity relative to the $n = 1$ IPS or increases in binding energy as the angle is increased as was observed in the phthalocyanine based monolayers. The small peak located halfway between the $n = 1$ and $n = 2$ IPS is attributed to an unoccupied metal surface state [45].

The H_2Pc and CoPc monolayer on Ag(111) substrate exhibit an increase in intensity for the $n = 2$ IPS around 13°. Though the spectra in Fig. 4 are normalized for viewing, the intensity increase persists on proper normalization to the electric field strength perpendicular to the sample. This intensity pattern is attributed to the slight extension of the projected bulk band gap below the Fermi level at the $\bar{\Gamma}$ point [46], which in conjunction with the requirement that the pump pulse is kept below the sample work function, limits the initial states to being non-$k_{||}$ conserving indirect transitions. As the sample is rotated away from the $\bar{\Gamma}$ point, the valence-band edge disperses strongly upwards (much greater than the IPS) and direct, $k_{||}$ conserving transitions, become possible before the $n = 2$ IPS disperses above the vacuum level. Further confirmation of this assignment comes from the lack of this spectral signature in the Ag(100) data.

In order to quantify the dispersions, the effective mass m^* for the $n = 1$ and $n = 2$ states was extracted by fitting the peak center versus $k_{||}$ to a parabola from 0.0 to 0.15 $Å^{-1}$. Higher lying IPS rapidly dispersed above the vacuum level, making the effective mass extraction unsuccessful. The effective mass in almost all cases was >1, with the exception of the CoPc/Ag(111) interface. In addition to the effective mass (m^*), the bandwidth (β) of the $n = 1_A$ state, and the band gap (Δ) between the $n = 1_A$ and $n = 1_B$ states was determined. The values are summarized in Table I.

IV. DISCUSSION AND MODELLING

The work functions for all of the phthalocyaine/Ag systems studied here are quite similar between 4.14 and 4.19 eV, within the error of the one-photon photoemission measurements. This observation itself is somewhat surprising. Previous studies have observed that there is a large charge transfer from the silver surface to the metal center in CoPc monolayers [32,33,40,42,43]. This mechanism cannot be operative in the case of H_2Pc, however, because it lacks the transition metal center. Instead, for the H_2Pc systems, charge transfer would need to occur into the ligand orbitals [36]. If these work functions are compared to the work functions of alkane/Ag(111) and Xe/Ag(111), which are surfaces not known to have charge transfer interactions, it is found that the phthalocyanines have

TABLE I. Dispersion parameters extracted from angle-resolved TPPE data. The m^* values are in units of m_e. The parameters Δ and β are the band gap and band width of the $n = 1$ IPS, respectively.

	$m^*_{n=1}$	$m^*_{n=2}$	Δ (meV)	β (meV)
H_2Pc/Ag(100)	1.39 ± 0.14	1.19 ± 0.16	252 ± 30	77 ± 30
H_2Pc/Ag(111)	1.43 ± 0.11	1.10 ± 0.10	268 ± 30	85 ± 30
CoPc/Ag(100)	1.30 ± 0.15	1.18 ± 0.10	162 ± 30	126 ± 30
CoPc/Ag(111)	1.00 ± 0.20	1.10 ± 0.15	161 ± 30	151 ± 30

work functions <150 meV higher than these cases. Using the Helmholtz work function equation, the resulting dipole is <1 Debye, which suggests only a fraction of an electron net charge transfer. This contrasts with the expected behavior for a sizable charge transfer to the cobalt metal center, and it implies that a more complex redistribution of charge must be taking place, which likely involves the ligand orbitals as has been reported previously [40]. This type of complex charge redistribution involving donation and back donation has been noted before [47–49].

Overall, the TPPE spectra look qualitatively the same as the FePc/Ag(111), CuPc/Ag(111), and PbPc/HOPG monolayers studied previously with TPPE [21,22], with a few small differences. In agreement with the previous studies, the two most strongly bound states are assigned to the $n = 1_A$ IPS state and the $n = 1_B$ IPS, which is "folded" via its interaction with the phthalocyanine lattice.

Previous work assigned the state at ∼0.2-eV binding energy to higher order folding of the $n = 1$ IPS. This assignment was primarily based on the lack of the observation of the higher lying IPS. However, in this study, we directly observe these higher states and thus assigned the peak at 0.2-eV BE to the $n = 2$ IPS. We suggest that the previous study [21] had more disorder as suggested by the broader LEED spots and more diffuse background resulting in shorter lifetimes and lower signal to noise that obscured the higher IPS.

A. One-dimensional modeling

The binding energies of the first three IPS are shown in Fig. 3(c). It can be immediately noted that the $n = 1$ IPS is more strongly bound than would be expected for an image potential state that strictly follows the commonly used quantum defect formula. Although there exist some surfaces for which a negative quantum defect can be explained by bulk band structure effects [50], in the case of silver, this is not the case. Thus the increase in image potential state binding energy must be due to the molecular film. This increased binding energy has been noted previously for similar systems [51] but its cause remains an open question.

The interaction between the molecular film and the IPS has previously been modeled with the electron affinity model [52]. In this model, the molecule is treated as a uniform dielectric of finite thickness on top of the metal surface. The potential is parameterized by the dielectric constant and electron affinity for the molecule, and is calculated classically. This model has proven successful for systems with negative electron affinities—e.g., systems where the dielectric material repels the electronic wave functions—however, the electron affinity model has proven less useful for systems with positive electron affinities such as phthalocyanines, which are predicted to pull the electronic wave function into the film. The obvious issue in applying this model in many systems is that it is undetermined how to select which unoccupied electronic state should be used as the electron affinity level in the model. An additional problem with the model is that it does not explicitly account for the substrate band structure, which plays a key role in determining the IPS binding energies.

Several groups have developed methods that successfully introduce the band structure of the substrate into the electron affinity model [52–55]. The method used here follows the work by Zhu *et al.* where the potential was split into two distinct regions [55]. The region inside the substrate is given by the Chulkov potential [56], which yields accurate binding energies for the electronic structure of the clean surface. While this model has no free parameters, the A_{10} parameter was adjusted to account for the change in work function upon adsorption of the phthalocyanine lattice. The region outside the substrate is given by the electron affinity model which takes the dielectric constant and electron affinity of the adlayer into account. Though finding an accurate measure of the dielectric constant for the phthalocyanine systems was difficult, a theoretical estimate [57] suggested a value of $\epsilon = 3.4$, which is in the range of the values used is previous studies [51,58]. The electron affinity of the film was left as a fitting parameter, because the proper value in materials with multiple unoccupied states below the vacuum level is ill-defined. The electron affinity in the present context should be viewed as an empirical construct necessary to model the effective interfacial potential energy landscape, which is probed by the image potential states. Comparisons between these parameters in different systems should be treated with care as they will be sensitive to many details of the system and the computation. The last region of the potential is the connection region at the interface, which has no additional free parameters and serves to continuously connect the two halves of the potential using an exponential transfer function.

A wave packet propagation technique [59] was used to solve for the eigenvalues of the model potential. Using values of 0.55 and 0.69 eV for electron affinity, values of CoPc and H_2Pc, respectively, led to image potential state binding energies that matched up closely with experiment; these energies are shown in Fig. 3(c) as dotted red lines. The fact that a single electron affinity correctly predicts the binding energy on both substrates demonstrates that the difference in binding energies between the Ag(100) and Ag(111) systems is purely dictated by the band structure of the substrate and substantial differences in the electronic structure of the adsorbates is unlikely. To our knowledge, this is the first case where the binding energies of the $n = 1$ state in the presence of an adsorbate have been compared on two different faces of the same crystal and demonstrates the utility of this hybrid model. Further details on the calculations and the explicit form of the potentials that was used are available in Ref. [60].

The existence of a band gap in the $n = 1$ IPS signifies that the potential parallel to the interface is corrugated. Because this corrugation must be due to the phthalocyanine lattice it is localized near the surface plane and thus breaks the separability of the potential parallel and perpendicular to the interface, making attempts to model the full system difficult. Previous works have used multidimensional models that took both in-plane and out-of-plane potentials into account [16,61], but these studies used nongeneral forms for the interfacial potential making them difficult to extend to other systems such as those under study. The most recent modeling work on phthalocyanines has assumed separability for the $n = 1$ IPS and treated only the potential parallel to the interface using a periodic square well [21] or periodic delta function model [22], which cannot easily determine the binding energies relative to the vacuum level.

B. Two-dimensional modeling

Our goal is to construct a simple and general model that incorporates the essential physics and fully determines the peak dispersions in the measured spectra; this should allow comparison of the band folding phenomenon in different systems on an equal footing. To do this, we propose the following two-dimensional potential:

$$V_{2D}(x,z) = V_{Zhu}(z; EA(x)),$$
$$EA(x) = -EA_0 + \delta EA\ \cos(2\pi x/L).$$

Here, the potential is the same as used in the one-dimensional model, except that the effective electron affinity varies as a function of position within the plane of the surface, which is denoted by the coordinate x. This new x-dependent electron affinity is parameterized by EA_0 and δEA. The position dependent electron affinity is necessary to build the corrugated potential energy landscape into the model. The physical interpretation of this position dependent electron affinity parameter is only that the potential energy landscape is corrugated. In this work, we chose a sinusoidal dependence as opposed to square well or δ-function-based potentials because we believe that the nearly-free electron model [15] is the natural model to use for dispersive, IPS-derived states. This choice was further motivated by the discontinuities present in the latter potentials, which can cause numerical difficulties in calculations. This model was solved in the same manner as the one-dimensional model, with a wave packet propagation technique.

The calculations were performed assuming that the electronic structure of the adsorbate and corrugation of the potential was conserved between different metal surfaces. This is supported by the one-dimensional calculations that clearly showed the differences in binding energies could be predicted from band structure effects alone. In order to obtain a best fit to the experiment, we iteratively fit the EA_0 and δEA parameters for each molecule to the datasets on both crystal surfaces until absolute binding energies and dispersion bandwidths and band gaps were best fit. The resulting parameters are listed in Table II, and the fits to example data sets are shown in Fig. 5.

Though there is no absolute scale to judge the electron affinity parameters, they may be meaningfully compared to each other in the present work. A few things are immediately noticed. First, the effective electron affinities in the two-dimensional model are substantially less those in the one-dimensional model. This is to be expected since the sinusoidal term increases the binding energy as the δEA term is increased. In the one-dimensional model, the EA parameter of the H_2Pc was 140 meV larger than that of CoPc, while in the two-dimensional model, the EA_0 are identical within error of the fitting. The δEA values of 1.56 and 1.02 eV for the H_2Pc and CoPc are significantly different, showing that the CoPc interface experiences a lower degree of corrugation than the H_2Pc interface. This follows directly from the bandwidth, band gap, and effective mass measurements collected in Table I.

TABLE II. Electron affinity parameters used in the model potential calculations.

1D model	EA (eV)	
H_2Pc	0.69 ± 0.05	
CoPc	0.55 ± 0.05	
2D model	EA_0 (eV)	δEA (eV)
H_2Pc	0.30 ± 0.05	1.56 ± 0.18
CoPc	0.30 ± 0.05	1.02 ± 0.19

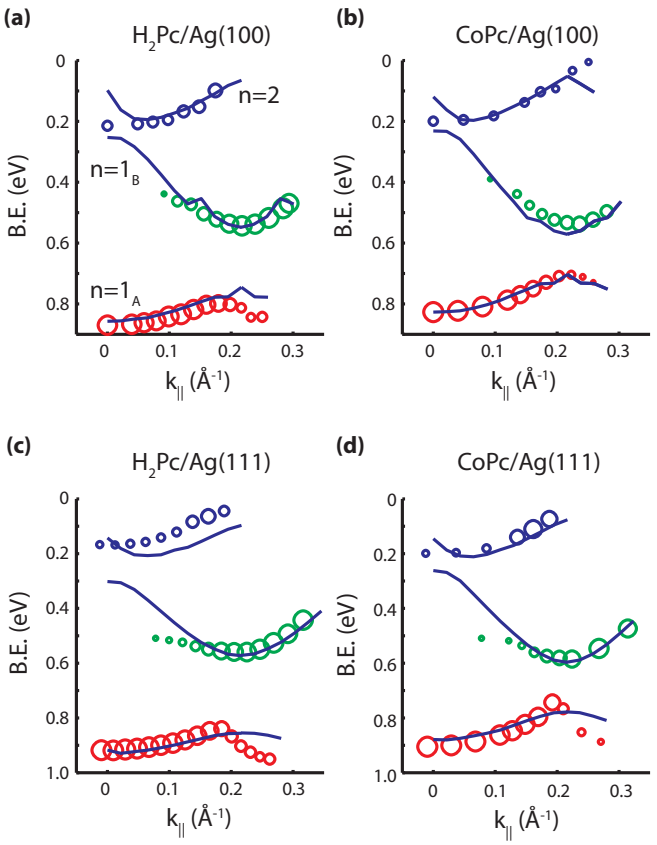

FIG. 5. (Color online) (a)–(d) Dispersions calculated with the two-dimensional model developed in the text are shown as blue lines. The circles are peak centers extracted from least squares fits to angular dispersion data. The size of the circles shows how the intensity of each band changes as a function of $k_{||}$.

Two details of the calculated dispersions are worth noting. First, our model predicts that the valence sp band of the Ag(100) should weakly back fold into the $n = 1_B$ IPS, causing the slight kink in the calculated dispersion, which was not observed in the data. This type of interaction is not well-described by the model used, and should not be regarded as meaningful. Additionally, the model shows an anti-crossing between the $n = 1_B$ and the $n = 2$ IPS near the $\bar{\Gamma}$ point in agreement with previous theoretical work on the stepped Cu(100) surface [61]. This would manifest in the data as a very heavy or negative effective mass for the $n = 2$ IPS near the $\bar{\Gamma}$ point. In all cases, the $n = 2$ effective mass was slightly heavier than that of a free electron which might suggest that the $n = 2$ IPS experienced some small degree of corrugation due to the molecular lattice, however, no direct evidence of this anticrossing was seen experimentally. Both the sp-band "kink" and the $n = 2$ IPS anticrossing result of an imperfect description of the interfacial potential due to the phthalocyanine lattice as expected from such a simple

model. Improving on this will likely require improvements to the current level of electronic structure theory available to surface scientists.

Comparing the Ag(111) and Ag(100) dispersions suggests that the symmetry of the substrate and resulting directions probed in k space also influences the spectra. In the case of Ag(100), the unit cell is square and the molecule is rotated only a few degrees ($\sim 15^\circ$) from having the same symmetry as the underlying surface [32]. On the Ag(111) surface, however, there are many symmetry equivalent domains due to the rotational symmetry of the substrate, hence the data collected will be averaged over many paths in k space. This can be qualitatively seen in Ag(111) data in Figs. 5(c) and 5(d) by noting the flatter dispersion of the $n = 1_B$ state, which is predicted for directions away from the $\bar{\Gamma}$-$\bar{M}$ directions in k space (with respect to the phthalocyanine Brillouin zone) as a consequence of the two-dimensional nature of the surface plane [21]. That the Ag(100) system fits better to the current model suggests that the anisotropy in the two-dimensional dispersion plays a role in determining the Ag(111) dispersion. In general, it can be expected that the fewer the rotational domains present, the better the dispersions should fit to the model presented here.

Finally, we recall the peak that grows in at small binding energies ($\sim$0.2 eV) and at very high angles in all the phthalocyanine spectra. Previous work assigned this peak to a high order back folding of the $n = 1$ IPS [21]. This mechanism is likely operative in these samples as well, though clear interpretation of this peak is significantly hindered by the range of angles accessible in our experimental setup. The model presented here did not predict this state, but this is expected because it only treats a single dimension parallel to the surface in contrast to the previous work. Further work will be required to understand the origin of this peak more fully.

C. Proposed origins of band folding

Though we have answered several questions regarding the nature of the band folding seen in phthalocyanine systems, there remains the question: what is causing the difference in corrugation between H_2Pc and CoPc at the interface? To discuss possible reasons, we must first discuss the origin of the band folding phenomenon itself.

Previous work has noted band folding in several systems, but generally its cause has not been discussed in detail. In previous work, geometric corrugation caused by step edges (vicinal surfaces) [20], molecular shape (C_{60}) [16], complex unit cells (benzene) [18], or moiré patterns (graphene) [62] was cited to account for the measured dispersions, but these mechanisms are not at work in the present case. In the case of C_{60}/Cu(111) [16], a sizable (2e) charge transfer to the hollow C_{60} molecules created a periodic array of point charges, strongly corrugating the interface and decreasing the bandwidth of the $n = 1$ IPS, but again this mechanism does not seem to be operative in this case; the relatively low work functions and similarity in the observed spectra for the CoPc and H_2Pc do not support it. Lacking obvious mechanisms, we chose to ask the question of whether or not crystallinity and lattice constant were enough to cause the corrugation of the potential in polycyclic aromatic hydrocarbon systems; perhaps the σ bonds, intermolecular spacing, and π system is enough to cause the effect. This is easily tested by comparing the PTCDA/Ag(100) interface to the phthalocyanine systems in Fig. 4. No peak is seen to grow in and disperse to lower binding energies as a function of angle, and thus no peak is assignable as a $n = 1_B$ state. This comparison clearly shows that the explanation of the band folding in phthalocyanine systems goes beyond having a lattice constant on the correct length scale or a high level of crystallinity as demonstrated in the measured LEED patterns in Fig. 2. We note that although our experiments did not show crystallinity to be sufficient for band folding to be observed, we do believe it is necessary since disorder in the phthalocyanine monolayer (as measured with LEED) caused the spectoscopic signatures of band folding to disappear, e.g., the spectra for the disordered phthalyanine layers did not show a clear $n = 1_B$ state, or have well-defined bandwidths or bandgaps.

In order to explain the strong band folding induced by the phthalocyanine lattice, previous work has appealed to the idea of hybridization of the IPS with an unoccupied molecular state [21,22]. This mechanism is attractive, but the energetic location and nature of the unoccupied states of phthalocyanine/metal interfaces is still a matter of investigation making an unambiguous assignment difficult. Additionally, although theoretical descriptions of how this type of hybridization might occur have become viable for some cases [63,64], they have not been generalized in a way that can be used in the current situation. Thus although the description relying on a quantum mechanical hybridization of molecular states and IPS is undoubtedly the most accurate, its lack of practical utility motivates us to offer an alternate perspective.

Thus, instead of invoking a hybridization model, we choose to appeal to chemical intuition. Figure 6(a) shows a H_2Pc molecule on a Ag(100) surface in a 5×5 unit cell. Figure 6(b) shows a contour plot of the electrostatic potential 1.5 Å above the molecular plane calculated at the plane-wave density functional theory level [65]. The most prominent feature of this contour plot is the appearance of repulsive areas near the nonprotonated nitrogen atoms. This is due to the electron density of the nitrogen lone pairs and has recently been directly

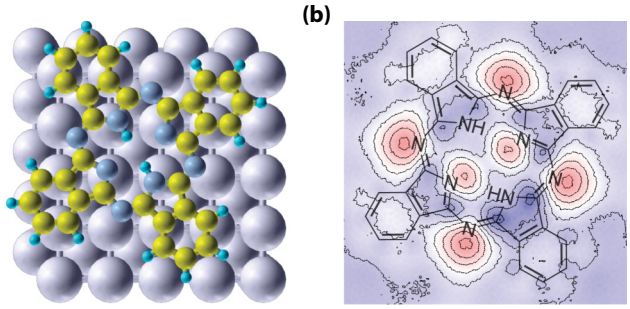

FIG. 6. (Color online) (a) A H_2Pc molecule on Ag(100) in a 5×5 unit cell. Color scheme: Ag is gray, C is yellow, N is blue, H is cyan. (b) The electrostatic potential at 1.5 Å above the molecular plane. The red areas near the nitrogen atoms represent areas of higher potential energy for an electron relative to the rest of the potential energy landscape, which is predominately colored blue. These images were created using the XCRYSDEN software.

imaged in kelvin probe force microscopy experiments [66]. Thus we propose that these nitrogen lone pair orbitals may be the reason that the phthalocyanine systems seem to experience a larger corrugation of the interfacial potential than other organic molecules. This can also be used to speculate as to the reason that the CoPc system is less strongly corrugated than the H_2Pc. In the CoPc system, the lone pairs in the center region are donated to the metal center, which should serve to screen the charge and smooth out the interfacial potential. Future experiments on the porphyrin analog to the phthalocyanine that lacks the bridging nitrogen atoms should lend further insight into this matter.

Finally, we point to a potential connection between our TPPE experiments and recent photoemission experiments [24–26]. In these photoemission experiments, it was observed that the molecular lattice present at the surface seemed to serve as a two-dimensional transmission grating, efficiently scattering the electrons as they transmitted the surface towards the detector. This phenomenon is known as surface umklapp scattering and couples the outgoing electron's wave vector to the lattice wave vector and alters the resulting photoemission spectra in sometimes misleading ways [24]. This mechanism is distinguished from the statically modified band structure we measure in the TPPE experiments, though we believe that both phenomena have the same origin. In order to understand this scattering process more fully, a quantitative theoretical description will be needed, and this necessitates the development of a suitable potential energy function to describe the interface. We believe our TPPE experiments and subsequent modeling more directly probe this interfacial potential due to high overlap between the image potential states and the potential in question, and we suggest that the model potential we have derived may be useful in modeling these scattering phenomena.

V. SUMMARY AND CONCLUSIONS

The present results expand the understanding of how band-folding manifests in TPPE spectra, which will be helpful in interpreting complex spectra taken on large aromatic monolayer systems. The phthalocyanine ligand is found to strongly perturb the interfacial potential and cause a sizable splitting of the $n = 1$ IPS band. Though the first image potential state is strongly modified by the corrugated potential it was found that the higher lying states of the Rydberg series were intact. Comparing the H_2Pc and CoPc data it was determined that the band folding was primarily due to the phthalocyanine ligand and the presence of a metal center actually smoothed the corrugation in contrast with the simple expectation that the electron dense metal atom would serve as an efficient scattering center. It was proposed that the nitrogen lone pairs may be important in determining the interfacial potential.

Experiments on the Ag(111) and Ag(100) crystals enabled several interesting observations. First using a simple model potential the different binding energies for the $n = 1$ IPS' on the two crystal could be explained from bulk band structure effects. To the authors' knowledge, this is the first time a comparison like this has been demonstrated with an organic adsorbate. Additionally, the shape of the Ag(111) and Ag(100) dispersions differed only slightly and these differences were attributed to the averaging over rotational domains in the case of Ag(111).

In an attempt to develop a practical model of band folding, we constructed a model that takes both the band structure and molecular lattice into account. This model adequately fit the spectra and allowed the extraction of the strength of the interfacial corrugation. The model is general and should be applicable to future systems, enabling the comparison of corrugation strengths.

As TPPE is applied to more and more complex systems, the interpretation of the spectra will become more difficult. It is our hope that the present data and proposed model will enable more accurate modeling of the effects of lattice corrugation on the IPS' that are ubiquitous at the metal/molecule interface.

ACKNOWLEDGMENTS

This work was supported by the Director, Office of Science, Office of Basic Energy Sciences, Chemical Sciences Division of the U.S. Department of Energy, under Contract No. DE-AC02-05CH11231.

[1] J. Hwang, A. Wan, and A. Kahn, Mater. Sci. Eng., R **64**, 1 (2009).
[2] S. Braun, W. R. Salaneck, and M. Fahlman, Adv. Mater. **21**, 1450 (2009).
[3] J. C. Scott, J. Vac. Sci. Technol. A **21**, 521 (2003).
[4] H. Ishii, K. Sugiyama, E. Ito, and K. Seki, Adv. Mater. **11**, 605 (1999).
[5] R. M. Osgood, Jr. and X. Wang, Solid State Phys. **51**, 1 (1997).
[6] R. W. Schoenlein, J. G. Fujimoto, G. L. Eesley, and T. W. Capehart, Phys. Rev. Lett. **61**, 2596 (1988).
[7] P. Echenique, J. Pitarke, E. Chulkov, and V. Silkin, J. Electron Spectrosc. **126**, 163 (2002).
[8] U. Bovensiepen, Prog. Surf. Sci. **78**, 87 (2005).
[9] N. Ge, Science **279**, 202 (1998).
[10] A. D. Miller, I. Bezel, K. J. Gaffney, S. Garrett-Roe, S. H. Liu, P. Szymanski, and C. B. Harris, Science **297**, 1163 (2002).
[11] J. Güdde, M. Rohleder, T. Meier, S. W. Koch, and U. Höfer, Science **318**, 1287 (2007).
[12] J. D. McNeill, R. L. Lingle, N.-H. Ge, C. M. Wong, R. E. Jordan, and C. B. Harris, Phys. Rev. Lett. **79**, 4645 (1997).
[13] M. Rohleder, W. Berthold, J. Güdde, and U. Höfer, Phys. Rev. Lett. **94**, 017401 (2005).
[14] M. Weinert, S. L. Hulbert, and P. D. Johnson, Phys. Rev. Lett. **55**, 2055 (1985).
[15] N. W. Ashcroft and N. D. Mermin, *Solid State Physics* (Saunders College, Philadelphia, 1976).
[16] G. Dutton, J. Pu, D. G. Truhlar, and X.-Y. Zhu, J. Chem. Phys. **118**, 4337 (2003).

[17] X.-Y. Zhu, G. Dutton, D. P. Quinn, C. D. Lindstrom, N. E. Schultz, and D. G. Truhlar, Phys. Rev. B **74**, 241401 (2006).

[18] D. Velic, A. Hotzel, M. Wolf, and G. Ertl, J. Chem. Phys. **109**, 9155 (1998).

[19] C. H. Schwalb, S. Sachs, M. Marks, A. Schöll, F. Reinert, E. Umbach, and U. Höfer, Phys. Rev. Lett. **101**, 146801 (2008).

[20] M. Roth, M. Pickel, J. Wang, M. Weinelt, and T. Fauster, Appl. Phys. B **74**, 661 (2002).

[21] E. A. Muller, J. E. Johns, B. W. Caplins, and C. B. Harris, Phys. Rev. B **83**, 165422 (2011).

[22] R. Yamamoto, T. Yamada, M. Taguchi, K. Miyakubo, H. S. Kato, and T. Munakata, Phys. Chem. Chem. Phys. **14**, 9601 (2012).

[23] Z. Zhang, H. Huang, X. Yang, and L. Zang, J. Phys. Chem. Lett. **2**, 2897 (2011).

[24] L. Giovanelli, F. C. Bocquet, P. Amsalem, H.-L. Lee, M. Abel, S. Clair, M. Koudia, T. Faury, L. Petaccia, D. Topwal, E. Salomon, T. Angot, A. A. Cafolla, N. Koch, L. Porte, A. Goldoni, and J.-M. Themlin, Phys. Rev. B **87**, 035413 (2013).

[25] L. Giovanelli, P. Amsalem, T. Angot, L. Petaccia, S. Gorovikov, L. Porte, A. Goldoni, and J.-M. Themlin, Phys. Rev. B **82**, 125431 (2010).

[26] F. C. Bocquet, L. Giovanelli, P. Amsalem, L. Petaccia, D. Topwal, S. Gorovikov, M. Abel, N. Koch, L. Porte, A. Goldoni, and J.-M. Themlin, Phys. Rev. B **84**, 241407 (2011).

[27] J. Ikonomov, O. Bauer, and M. Sokolowski, Surf. Sci. **602**, 2061 (2008).

[28] R. Lingle, N.-H. Ge, R. Jordan, J. McNeill, and C. Harris, Chem. Phys. **205**, 191 (1996).

[29] W. Steinmann, Phys. Status Solidi B **192**, 339 (1995).

[30] W. Steinmann and T. Fauster, *Photonic Probes of Surfaces*, edited by P. Halevi (Elsevier, Amsterdam, 1995), Vol. 2 .

[31] W. Dou, Y. Tang, C. S. Lee, S. N. Bao, and S. T. Lee, J. Chem. Phys. **133**, 144704 (2010).

[32] A. Mugarza, R. Robles, C. Krull, R. Korytár, N. Lorente, and P. Gambardella, Phys. Rev. B **85**, 155437 (2012).

[33] E. Salomon, P. Amsalem, N. Marom, M. Vondracek, L. Kronik, N. Koch, and T. Angot, Phys. Rev. B **87**, 075407 (2013).

[34] J. D. Baran and J. A. Larsson, J. Phys. Chem. C **117**, 23887 (2013).

[35] S. Kera, M. Casu, K. Bauchspieß, D. Batchelor, T. Schmidt, and E. Umbach, Surf. Sci. **600**, 1077 (2006).

[36] I. Kröger, P. Bayersdorfer, B. Stadtmüller, C. Kleimann, G. Mercurio, F. Reinert, and C. Kumpf, Phys. Rev. B **86**, 195412 (2012).

[37] I. Kröger, B. Stadtmüller, C. Stadler, J. Ziroff, M. Kochler, A. Stahl, F. Pollinger, T.-L. Lee, J. Zegenhagen, F. Reinert, and C. Kumpf, New J. Phys. **12**, 083038 (2010).

[38] C. Stadler, S. Hansen, I. Kröger, C. Kumpf, and E. Umbach, Nat. Phys. **5**, 153 (2009).

[39] T. G. Gopakumar, T. Brumme, J. Kroger, C. Toher, G. Cuniberti, and R. Berndt, J. Phys. Chem. C **115**, 12173 (2011).

[40] M. Toader, P. Shukrynau, M. Knupfer, D. R. T. Zahn, and M. Hietschold, Langmuir **28**, 13325 (2012).

[41] K. Manandhar, T. Ellis, K. Park, T. Cai, Z. Song, and J. Hrbek, Surf. Sci. **601**, 3623 (2007).

[42] M. Schmid, A. Kaftan, H.-P. Steinrück, and J. M. Gottfried, Surf. Sci. **606**, 945 (2012).

[43] F. Petraki, H. Peisert, F. Latteyer, U. Aygül, A. Vollmer, and T. Chassé, J. Phys. Chem. C **115**, 21334 (2011).

[44] M. Marks, C. H. Schwalb, K. Schubert, J. Güdde, and U. Höfer, Phys. Rev. B **84**, 245402 (2011).

[45] M. C. E. Galbraith, M. Marks, R. Tonner, and U. Höfer, J. Phys. Chem. Lett. **5**, 50 (2014).

[46] S. D. Kevan and R. H. Gaylord, Phys. Rev. B **36**, 5809 (1987).

[47] L. Romaner, G. Heimel, J.-L. Brédas, A. Gerlach, F. Schreiber, R. L. Johnson, J. Zegenhagen, S. Duhm, N. Koch, and E. Zojer, Phys. Rev. Lett. **99**, 256801 (2007).

[48] P. S. Bagus, D. Käfer, G. Witte, and C. Wöll, Phys. Rev. Lett. **100**, 126101 (2008).

[49] S. Lindner, U. Treske, and M. Knupfer, Appl. Surf. Sci. **267**, 62 (2013).

[50] V. M. Silkin, E. V. Chulkov, and P. M. Echenique, Phys. Rev. B **60**, 7820 (1999).

[51] C. D. Lindstrom, M. Muntwiler, and X. Y. Zhu, J. Phys. Chem. B **111**, 6913 (2007).

[52] J. D. McNeill, R. L. Lingle, R. E. Jordan, D. F. Padowitz, and C. B. Harris, J. Chem. Phys. **105**, 3883 (1996).

[53] D. C. Marinica, C. Ramseyer, A. G. Borisov, D. Teillet-Billy, J. P. Gauyacq, W. Berthold, P. Feulner, and U. Hofer, Phys. Rev. Lett. **89**, 046802 (2002).

[54] W. Berthold, F. Rebentrost, P. Feulner, and U. Höfer, Appl. Phys. A **78**, 131 (2004).

[55] C. D. Lindstrom, D. Quinn, and X.-Y. Zhu, J. Chem. Phys. **122**, 124714 (2005).

[56] E. Chulkov, V. Silkin, and P. Echenique, Surf. Sci. **437**, 330 (1999).

[57] N. Shi and R. Ramprasad, Appl. Phys. Lett. **89**, 102904 (2006).

[58] C. H. Schwalb, M. Marks, S. Sachs, A. Schöll, F. Reinert, E. Umbach, and U. Höfer, Eur. Phys. J. B **75**, 23 (2010).

[59] E. V. Chulkov, A. G. Borisov, J. P. Gauyacq, D. Sanchez-Portal, V. M. Silkin, V. P. Zhukov, and P. M. Echenique, Chem. Rev. **106**, 4160 (2006).

[60] See Supplemental Material at http://link.aps.org/supplemental/10.1103/PhysRevB.89.155422 for the details of the model potentials and wave packet propagation technique.

[61] J. Lei, H. Sun, K. W. Yu, S. G. Louie, and M. L. Cohen, Phys. Rev. B **63**, 045408 (2001).

[62] N. Armbrust, J. Güdde, P. Jakob, and U. Höfer, Phys. Rev. Lett. **108**, 056801 (2012).

[63] M. Feng, J. Zhao, T. Huang, X. Zhu, and H. Petek, Acc. Chem. Res. **44**, 360 (2011).

[64] N. L. Zaitsev, I. A. Nechaev, P. M. Echenique, and E. V. Chulkov, Phys. Rev. B **85**, 115301 (2012).

[65] P. Giannozzi, S. Baroni, N. Bonini, M. Calandra, R. Car, C. Cavazzoni, D. Ceresoli, G. L. Chiarotti, M. Cococcioni, I. Dabo, A. Dal Corso, S. de Gironcoli, S. Fabris, G. Fratesi, R. Gebauer, U. Gerstmann, C. Gougoussis, A. Kokalj, M. Lazzeri, L. Martin-Samos, N. Marzari, F. Mauri, R. Mazzarello, S. Paolini, A. Pasquarello, L. Paulatto, C. Sbraccia, S. Scandolo, G. Sclauzero, A. P. Seitsonen, A. Smogunov, P. Umari, and R. M. Wentzcovitch, J. Phys. Condens. Matter **21**, 395502 (2009).

[66] F. Mohn, L. Gross, N. Moll, and G. Meyer, Nat. Nanotechnol. **7**, 227 (2012).